

Sensitivity analysis for finite element modeling of humeral bone and cartilage

Bola, Ana M.¹, Ramos, A.^{*1} and Simões, J. A²

¹*Biomechanics Research Group, TEMA, University of Aveiro, 3810-193 Aveiro, Portugal*

²*High School of Arts and Design, Avenida Calouste Gulbenkian, Matosinhos, Portugal*

(Received January 10, 2016, Revised March 28, 2016, Accepted March 29, 2016)

Abstract. The finite element method is wide used in simulation in the biomechanical structures, but a lack of studies concerning finite element mesh quality in biomechanics is a reality. The present study intends to analyze the importance of the mesh quality in the finite element model results from humeral structure. A sensitivity analysis of finite element models (FEM) is presented for the humeral bone and cartilage structures. The geometry of bone and cartilage was acquired from CT scan and geometry reconstructed. The study includes 54 models from same bone geometry, with different mesh densities, constructed with tetrahedral linear elements. A finite element simulation representing the glenohumeral-joint reaction force applied on the humerus during 90° abduction, with external load as the critical condition. Results from the finite element models suggest a mesh with 1.5 mm, 0.8 mm and 0.6 mm as suitable mesh sizes for cortical bone, trabecular bone and humeral cartilage, respectively. Relatively to the higher minimum principal strains are located at the proximal humerus diaphysis, and its highest value is found at the trabecular bone neck. The present study indicates the minimum mesh size in the finite element analyses in humeral structure. The cortical and trabecular bone, as well as cartilage, may not be correctly represented by meshes of the same size. The strain results presented the critical regions during the 90° abduction.

Keywords: bone; humerus behavior; finite element analysis; mesh convergence; strain.

1. Introduction

The finite element method is wide used in simulation of biomechanical structures, including complex geometries, interactions between structures and mechanical properties of bones. The modelling of human articulations began by focusing mostly on the hip and knee than on the shoulder due to clinical aspects and to shoulder joint complexity.

Despite the continuous increase in hip and knee arthroplasties, (Australian Orthopaedic Association 2013), shoulder arthroplasty records are growing (New Zealand Joint Registry 2013) and, by 2015, its demand is expected to exceed that of hip and knee in the United States (Day *et al.* 2010). This growth has helped to turn the attention of researchers into the shoulder joint, as better prosthesis is a demand to correctly provide pain relief and reduce revision burden.

*Corresponding author, Professor, E-mail: a.ramos@ua.pt

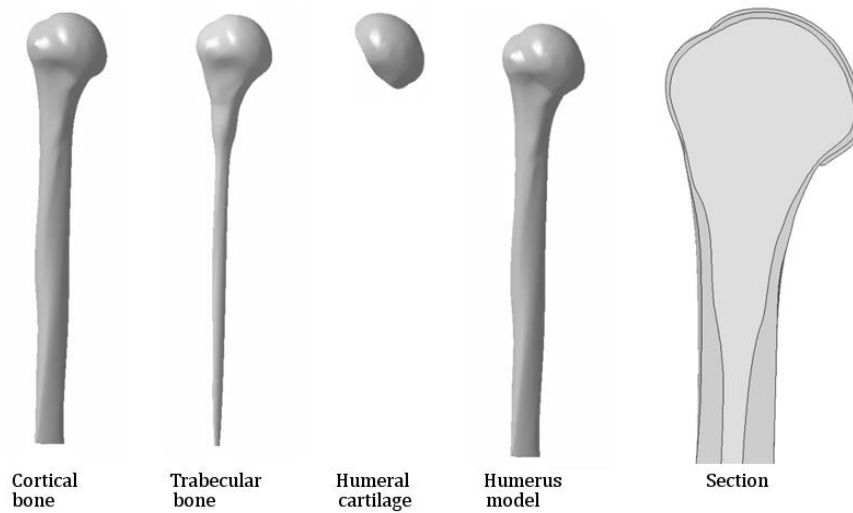


Fig. 1 Humeral Bone and cartilage models

Regardless of the growing number of studies using finite element models (FEM) in shoulder biomechanics (Favre *et al.* 2012; Hwang *et al.* 2014; Maldonado *et al.* 2003a; Metan *et al.* 2014; Varghese *et al.* 2011) or shoulder prosthesis (Gupta *et al.* 2004; Hopkins *et al.* 2006; Quental *et al.* 2012; Yongpravat *et al.* 2013), Burkhart *et al.* (2013) claim, in a recent review article, that there is a clear lack of studies concerning mesh quality, energy balance and validation methods in this field of studies. The importance of type of elements in the finite element models was analyzed previously and presented the importance of this factor in the results (Burkhart, 2013; Ramos and Simões, 2006). Another important point of the finite element models in the last 40th decades of analysis in biomechanics is the validation of models (Taylor and Prendergast, 2015), and the importance of the models accuracy to represent the real world variability. Since FEM of human features must be as accurate as possible, importance to mesh sensitivity analysis needs to be given when the validation of models is difficult or impossible. Other important factor in the finite element model simulation is the boundary conditions to represent the real scenario, and then the most critical situation should be considered in the analysis.

Therefore, the purpose of this study was focused on mesh sensitivity analysis of cortical and trabecular humeral bones and of humeral head cartilage. Stain distributions due to a 90° shoulder abduction were also determined as considered the most critical situation for the articulation.

2. Materials and methods

2.1 CAD model

A fourth generation composite left humerus model from Sawbones® was scanned with a Roland PicZa 3D Laser Scanner (resolution (1.4×1.4) mm). The external surface acquired was adapted with CATIA® (V5.21© Dassault Systèmes) (Relvas *et al.* 2011). The model of the humeral external geometry was obtained and a volume generated. The cortical thickness of the

Table 1 Material properties

	Cortical bone	Trabecular bone	Cartilage
Young Modulus	16.5 GPa (Varghese <i>et al.</i> 2011; Varghese <i>et al.</i> 2012)	124 MPa (Varghese <i>et al.</i> 2011)	0.66 MPa (Matsen <i>et al.</i> 1993)
Poisson ratio	0.3 (Varghese <i>et al.</i> , 2011)	0.3 (Varghese <i>et al.</i> 2011)	0.08 (Matsen <i>et al.</i> 1993)

proximal humerus has around 6 mm (Mather *et al.* 2013), while the cortical thickness of the humeral head has nearly 1.3 mm (Fox *et al.* 2008). The cortical bone structure was subtracted to the original body to create the trabecular bone volume. Regarding humeral cartilage, a constant thickness of 0.95 mm was assumed, being in accordance with literature (Fox *et al.* 2008; Yeh *et al.* 1998) and with the average observed in different CT scans. The CAD models after reconstruction and developed are presented in Fig. 1 as external and internal geometry.

2.2 Material properties

Bone and cartilage were considered isotropic linear elastic, similarly to other studies (Favre *et al.* 2012; Maldonado *et al.* 2003), and present good results in other bone structures in linear conditions. For trabecular bone, the relationship between Young's modulus and bone density was established (Varghese *et al.*, 2011). For the humeral head, bone density is the mean value of trabecular body mass density (Tingart *et al.* 2006). Humeral cartilage density equals glenoid cartilage density used by Gatii *et al.* (2010) on the development and validation of a FEM of the superior glenoid labrum. All material properties are presented in Table 1 and references of each work.

2.3 Finite element convergence analysis

FE meshes for cortical and trabecular bones and for cartilage were developed using CATIA® and analyzed independently from each other. In all meshes, the maximum gap between mesh and geometry was made equal to 0.5 mm. Eighteen models for each structure were constructed with

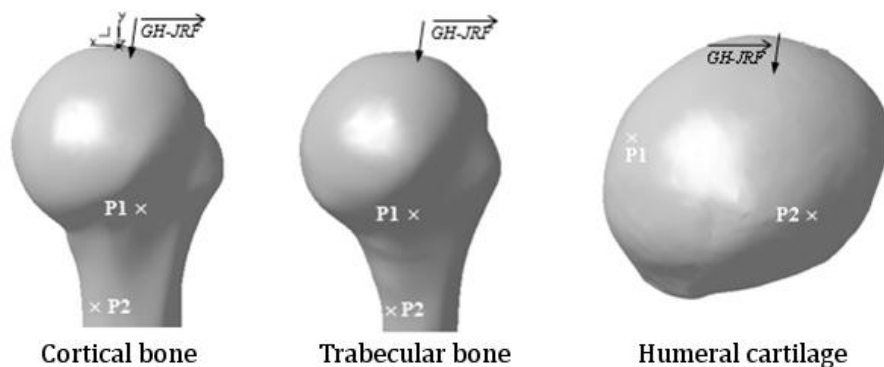


Fig. 2 GH-JRF and points analyzed

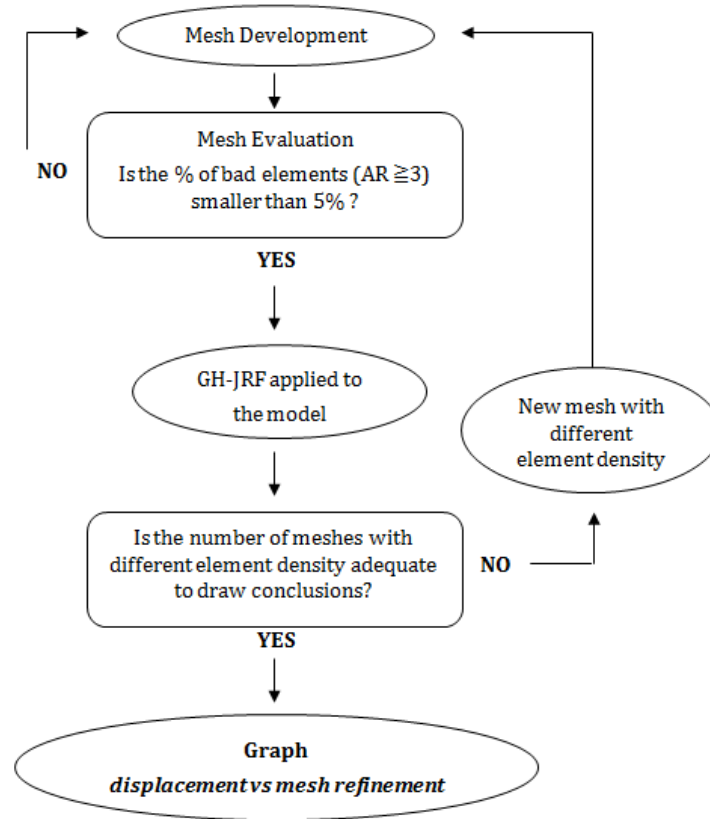


Fig. 3 Meshes selection process

different mesh densities. Tetrahedral linear elements, also used by others (Varghese *et al.* 2011), having three degrees of freedom per node, were chosen since they can be used under frictionless conditions (Tadepalli *et al.* 2011), as in the present case. Ramos and Simões (2006), on their study with a realistic model of a proximal femur, did not observe substantial differences between simulations obtained with first and second order tetrahedral and hexahedral elements. However, they verified that hexahedral quadratic elements appeared to be more stable and less influenced by mesh refinement.

To evaluate the created meshes, the average aspect ratio (AAR) and corresponding standard deviations (SD) were accessed. The criteria adopted to establish the degree of acceptance of the meshes considers that the percentage of elements with aspect ratio greater than 3 should remain below 5% (Burkhart *et al.* 2013).

The FEM of both bones were fixed distally, and the cartilage fixed laterally. For each mesh, compression tests were carried out simulating the application of a Glenohumeral Joint Reaction Force (GH-JRF) during 90° arm abduction with external load. GH-JRF was applied in a node at the top of the models and results were analyzed at two nodes in each model (see Fig. 2). The appropriate mesh sizes for each structure were then identified. A scheme procedure with the mesh selection process is represented in Fig. 3.

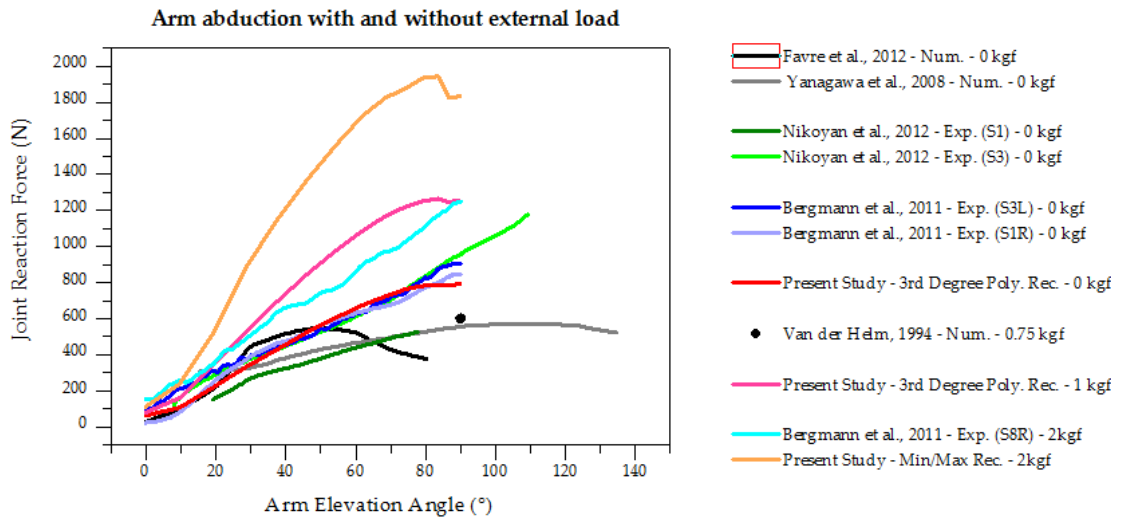


Fig. 4 Some GH-JRF in literature

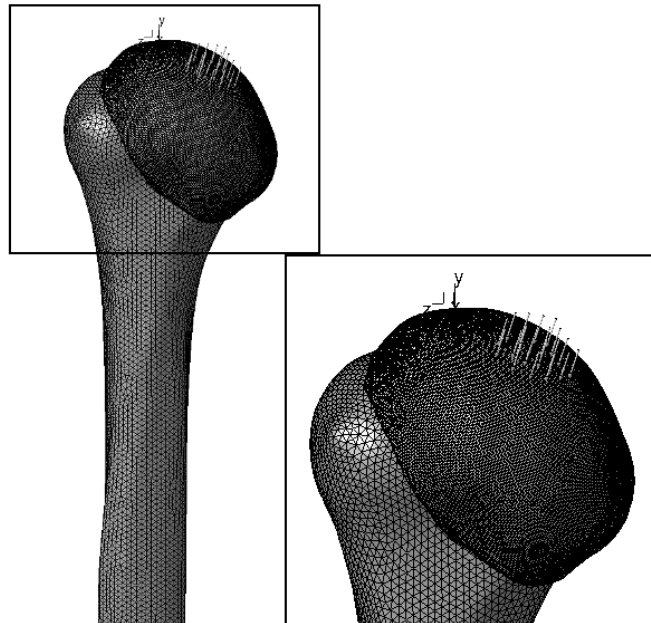


Fig. 5 GH-JRF applied to the humeral head during 90° abduction

GH-JRF was determined with AnyBody™ Modeling System (Version 5.0.0, 2014), a software specifically developed for musculoskeletal modelling analysis. It was concluded that with 2 kgf it is necessary more synergism between muscles to perform movement, and results were unsatisfactory when compared with literature (Bergmann *et al.* 2011).

Thus, an external load of 1 kgf was considered and the corresponding GH-JRF determined (472, -1250, 367) N, Cartesian coordinated system). GH-JRF is of the order of magnitude of

reaction forces determined by Bergmann *et al.* (2011) in their experiments with an instrumented shoulder prosthesis in forward flexion and abduction for patients holding an external load of 2 kgf (see Fig. 4) and suffering from osteoarthritis. It is important to note that anthropometry differences and shoulder osteoarthritis influence forces measured (Bergmann *et al.* 2011; Illyés and Kiss, 2005; Ludewig and Cook, 2000; Westerhoff *et al.* 2012).

2.4 Strain of the humerus during arm abduction

With the three appropriate mesh sizes identified, a new FEM was developed considering cortical and trabecular bones and cartilage. GH-JRF on the humerus during 90° abduction with external load of 1 kgf was applied as a distributed force. Its application area corresponds to the contact area between the humeral head and the glenoid (Sahara *et al.* 2007) (see Fig. 5). Cortical bone and trabecular bone meshes, and cortical bone and cartilage meshes share a common boundary and behave as a single body.

3. Results and discussion

3.1 Finite element convergence analysis

The number of elements, nodes and degrees of freedom (DOF), and the AAR and SD of each mesh are presented in Table IV, Table V and Table VI for cortical bone, trabecular bone and cartilage, respectively (see appendix). Tables present the percentage of good ($1 \leq AR \leq 2.5$), poor ($2.5 \leq AR < 3$) and bad ($AR \geq 3$) elements.

The AAR of all meshes are within the interval classified as good, with cartilage meshes presenting higher AARs. All cortical and trabecular bone meshes have a percentage of bad elements smaller than 5%. The same was not observed with humeral cartilage, since models with a mesh size of 2.5 mm and 3 mm present a percentage of bad elements of 7.7% and 14.6%, respectively, whereby these were not considered in the mesh refinement analysis.

Displacement results of cortical and trabecular bones are represented in graphs of Fig. 6.

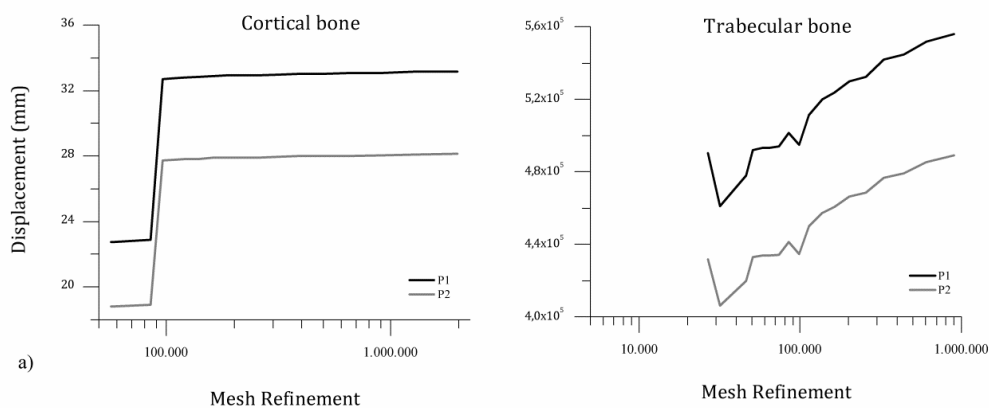


Fig. 6 Displacement versus mesh refinement, for a) cortical bone and b) trabecular bone

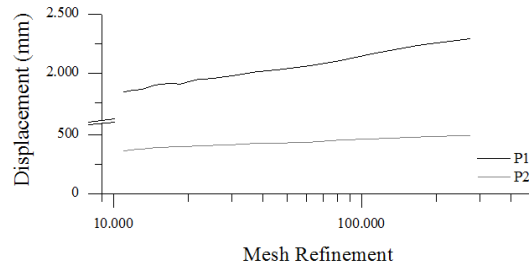


Fig. 7 Displacement versus mesh refinement for humeral cartilage

Table 2 FE mesh features of the final humeral model

Mesh	Mesh size (mm)	Elements		Nodes	NDOF	AAR (SD)
		Tetrahedral (% Good, % Poor, % Bad)	Spider			
Cortical bone	1.5	129,122 (89.7%, 7.6%, 2.7%)				1.773 (0.785)
Trabecular bone	0.8	150,917 (89.0%, 7.0%, 4.0%)	53,145	110,701	332,103	1.858 (0.858)
Cartilage	0.6	157,008 (99.8%, 0.03%, 0.00%)				1.442 (0.442)

For both bones, displacement at points P1 and P2 presents similar behavior. This means, on the one hand, that different regions of the same bone can be represented by the same mesh size. On the other hand, different bone types are represented by different meshes size. Regarding cartilage, displacement behavior is similar to those observed for bones, as exposed in graph of Fig. 7.

Mesh sizes of 1.5 mm, 0.8 mm and 0.6 mm are appropriate for modelling cortical bone, trabecular bone and cartilage, respectively, as they present small AARs. According to literature (Tsukerman and Plaks, 1998), the meshes have good quality to represent biomechanical behavior.

With the mesh sizes defined, a final FEM was developed with a total of 490,192 elements, 89.2% tetrahedral elements and 10.8% spider elements, employed in the connection between meshes. The model has 110,701 nodes and 332,103 DOF (see Table II).

In literature, there are many humerus and shoulder FE models devoted to study topics like bone remodeling (Quental *et al.* 2012), shoulder pathomechanics (Hwang *et al.* 2014), stress and strain distributions at the humerus (Maldonado *et al.* 2003; Varghese *et al.* 2011), glenohumeral stability (Favre *et al.* 2012) or osteoarthritic joints (Büchler *et al.*, 2002). Unfortunately, only few authors provide details on the developed meshes, and thus comparison of new models with existing ones is short. Nonetheless, some evaluations can be made.

In the study of Maldonado *et al.* (2003), bone is treated as inhomogeneous and CT density information is used. On the contrary, our model considers each bone structure as homogeneous and with higher Young Modulus. Nonetheless, both studies model bone as an isotropic linear elastic material. The other major difference between the two models relies on the type and number of elements used to build the FEM: only 58,048 eight-node brick elements were used by the authors.

Varghese *et al.* (2011), on a computed-tomography based FEM of long bones, used tetrahedral linear elements and made a convergence analysis. Element sizes of 2, 3 and 4 mm were evaluated and the authors consider 3 mm to be the optimal mesh size. However, on the basis of the mesh

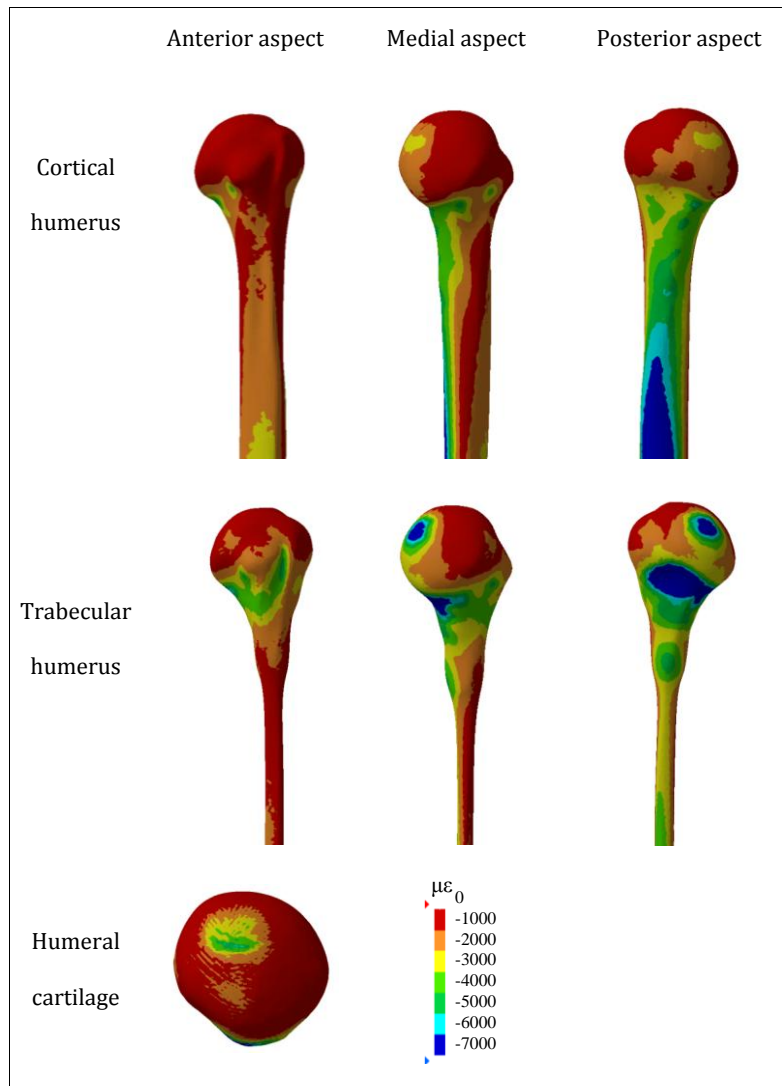


Fig. 8 Minimum principal strain patterns of cortical and trabecular humerus and humeral cartilage

convergence results of our study, a mesh size of 3 mm is considered large to correctly represent bone models geometry.

In yet another study (Favre *et al.* 2012), shoulder bone and cartilage models were developed with tetrahedral quadratic elements. Unfortunately, no details on mesh size, number of elements, nodes nor degrees of freedom are given and comparison cannot be accomplished.

3.2 Strain of the humerus during arm abduction

Minimum principal strain distributions at the humerus as consequence of the GH-JRF were determined (Fig. 8). The anterior, medial and posterior aspects of cortical and trabecular bone are shown, as well as of cartilage.

In a general way, results show that the minimum principal strain distributions are higher at the diaphysis than at the humeral head for both cortical and trabecular bone. Furthermore, strain in trabecular bone is higher than in cortical bone. In the humeral diaphysis, the anterior aspect presents higher strain values than the posterior, whereas strain distribution is similar between medial and lateral aspects. This behavior is also observed in both cortical and trabecular bones.

In the proximal part of the humerus, the highest principal strain value was found at the neck of trabecular bone (blue area evidenced in Fig.8, anterior aspect). These results indicate some correlation with in vivo situation, since in X-ray in this region presents higher bone density.

Concerning the humeral cartilage, it presents smaller strain distribution in all its area, excluding the extent where GH-JRF was applied.

Very few studies present the strain distribution at the proximal humerus are found in literature (Maldonado *et al.* 2003), and comparison with their results is difficult to accomplish due to different forces applied and material properties attributed.

4. Conclusions

The study presented intends to fill the gap established regarding mesh convergence analysis of FEM in biomechanics. It is focused on the humerus and considers cortical and trabecular bone and its cartilage. Results obtained suggest that mesh sizes depend on aspects like geometry and size of the surface or type of material attributed to the model. Thus, cortical and trabecular bone, as well as cartilage, may not be correctly represented by meshes of the same size. A drawback of the study is the lack of experimental validation, which is being planned for the next step.

Acknowledgments

This work was supported by the Fundação para a Ciência e a Tecnologia under grant number SFRH/BD/71162/2010.

References

- Australian Orthopaedic Association (2013), *National joint replacement registry*, Analysis of state & territory health data all arthroplasty. Supplementary Report 2013.
- Bergmann, G., Graichen, F., Bender, A., Rohlmann, A., Halder, A., Beier, A. and Westerhoff, P. (2011), "In vivo gleno-humeral joint loads during forward flexion and abduction", *J. Biomech.*, **44**(8), 1543-1552.
- Büchler, P., Ramaniraka, N.A., Rakotomanana, L.R., Iannotti, J.P. and Farron, A. (2002), "A finite element model of the shoulder: application to the comparison of normal and osteoarthritic joints", *Clinical Biomech.*, **17**(9), 630-639.
- Burkhart, T.A., Andrews, D.M. and Dunning, C.E. (2013), "Finite element modeling mesh quality, energy balance and validation methods: A review with recommendations associated with the modeling of bone tissue", *J. Biomech.*, **46**(9), 1477-1488.
- Day, J.S., Lau, E., Ong, K.L., Williams, G.R., Ramsey, M.L. and Kurtz, S.M. (2010), "Prevalence and projections of total shoulder and elbow arthroplasty in the United States to 2015", *J. Shoulder Elbow Surgery*, **19**(8), 1115-1120.
- Favre, P., Senteler, M., Hipp, J., Scherrer, S., Gerber, C. and Snedeker, J.G. (2012), "An integrated model of

- active glenohumeral stability”, *J. Biomech.*, **45**(13), 2248-2255.
- Fox, J.A., Cole, B.J., Romeo, A.A., Meininger, A.K., Williams, J.M., Glenn, R.E. and Dorow, C.B. (2008), “Articular cartilage thickness of the humeral head: an anatomic study”, *Orthopedics*, **31**(3), 216.
- Gatti, C.J., Maratt, J.D., Palmer, M.L., Hughes, R.E. and Carpenter, J.E. (2010), “Development and validation of a finite element model of the superior glenoid labrum”, *Ann. Biomed. Eng.*, **38**(12), 3766-3776.
- Gupta, S., Van der Helm, F.C.T. and Van Keulen, F. (2004), “Stress analysis of cemented glenoid prostheses in total shoulder arthroplasty”, *J. Biomech.*, **37**(11), 1777-1786.
- Hopkins, A.R., Hansen, U.N., Amis, A.A., Taylor, M., Gronau, N. and Anglin, C. (2006), “Finite element modelling of glenohumeral kinematics following total shoulder arthroplasty”, *J. Biomech.*, **39**(13), 2476-2483.
- Hwang, E., Carpenter, J.E., Hughes, R.E. and Palmer, M.L. (2014), “Shoulder labral pathomechanics with rotator cuff tears”, *J. Biomech.*, **47**(7), 1733-1738.
- Illyés, Á. and Kiss, R.M. (2005), “Shoulder muscle activity during pushing, pulling, elevation and overhead throw”, *J. Electromy. Kinesiol.*, **15**(3), 282-289.
- Ludewig, P.M. and Cook, T.M. (2000), “Alterations in shoulder kinematics and associated muscle activity in people with symptoms of shoulder impingement”, *Phys. Therapy*, **80**(3), 276-291.
- Maldonado, Z.M., Seebeck, J., Heller, M.O., Brandt, D., Hepp, P., Lill, H. and Duda, G.N. (2003), “Straining of the intact and fractured proximal humerus under physiological-like loading”, *J. Biomech.*, **36**(12), 1865-1873.
- Mather, J., MacDermid, J.C., Faber, K.J. and Athwal, G.S. (2013), “Proximal humerus cortical bone thickness correlates with bone mineral density and can clinically rule out osteoporosis”, *J. Shoulder Elbow Surgery*, **22**(6), 732-738.
- Matsen, F.A., (1993), *The Shoulder: A Balance of Mobility and Stability: workshop*, Vail, Colorado, September.
- Metan, S.S., Krishna, P. and Mohankumar, G.C. (2014), “FEM model an effective tool to evaluate von mises stresses in shoulder joint and muscles for adduction and abduction”, *Procedia Mater. Sci.*, **5**, 2090-2098.
- New Zealand Joint Registry (2013), *The New Zealand joint registry - fifteen year report - January 1999 to December 2013*.
- Quental, C., Folgado, J., Fernandes, P.R. and Monteiro, J. (2012), “Bone remodelling analysis of the humerus after a shoulder arthroplasty”, *Medical Eng. Phys.*, **34**(8), 1132-1138.
- Ramos, A. and Simoes, J.A. (2006), “Tetrahedral versus hexahedral finite elements in numerical modelling of the proximal femur”, *Medical Eng. Phys.*, **28**(9), 916-924.
- Relvas, C., Ramos, A., Completo, A. and Simões, J.A. (2011), “Accuracy control of complex surfaces in reverse engineering”, *Int. J. Precision Eng. Manufact.*, **12**(6), 1035-1042.
- Sahara, W., Sugamoto, K., Murai, M., Tanaka, H. and Yoshikawa, H. (2007), “The three-dimensional motions of glenohumeral joint under semi-loaded condition during arm abduction using vertically open MRI”, *Clinical Biomech.*, **22**(3), 304-312.
- Tadepalli, S.C., Erdemir, A. and Cavanagh, P.R. (2011), “Comparison of hexahedral and tetrahedral elements in finite element analysis of the foot and footwear”, *J. Biomech.*, **44**(12), 2337-2343.
- Taylor, M. and Prendergast, P.J. (2015), “Four decades of finite element analysis of orthopaedic devices: Where are we now and what are the opportunities?”, *J. Biomech.*, **48**(5), 767-778.
- Tingart, M.J., Lehtinen, J., Zurakowski, D., Warner, J.J. and Apreleva, M. (2006), “Proximal humeral fractures: regional differences in bone mineral density of the humeral head affect the fixation strength of cancellous screws”, *J. Shoulder Elbow Surgery*, **15**(5), 620-624.
- Tsukerman, I. and Plaks, A. (1998), “Comparison of accuracy criteria for approximation of conservative fields on tetrahedra”, *Proceedings of the IEEE transactions on magnetics*, **34**(5), 3252-3255.
- Varghese, B., Short, D. and Hangartner, T. (2012), “Development of quantitative computed-tomography-based strength indicators for the identification of low bone-strength individuals in a clinical environment”, *Bone*, **50**(1), 357-363.

- Varghese, B., Short, D., Penmetsa, R., Goswami, T. and Hangartner, T. (2011), "Computed-tomography-based finite-element models of long bones can accurately capture strain response to bending and torsion", *J. Biomech.*, **44**(7), 1374-1379.
- Westerhoff, P., Graichen, F., Bender, A., Halder, A., Beier, A., Rohlmann, A. and Bergmann, G. (2012), "In vivo measurement of shoulder joint loads during walking with crutches", *Clinical Biomech.*, **27**(7), 711-718.
- Yeh, L., Kwak, S., Kim, Y.S., Chou, D.S., Muhle, C., Skaf, A., ... and Resnick, D. (1998), "Evaluation of articular cartilage thickness of the humeral head and the glenoid fossa by MR arthrography: anatomic correlation in cadavers", *Skeletal radiol.*, **27**(9), 500-504.
- Yongpravat, C., Kim, H.M., Gardner, T.R., Bigliani, L.U., Levine, W.N. and Ahmad, C.S. (2013), "Glenoid implant orientation and cement failure in total shoulder arthroplasty: a finite element analysis", *J. Shoulder Elbow Surgery*, **22**(7), 940-947.

MC

Appendix

TABLE III- FE MESH FEATURES FOR CORTICAL BONE

Mesh size (mm)	Number of Elements	Number of Nodes	NDOF	% Of Elements			AAR (SD)
				Good ($1 \leq AR < 2.5$)	Poor ($2.5 \leq AR < 3$)	Bad ($AR \geq 3$)	
0.5	1,975,228	422,497	1,267,491	97.72	2.04	0.23	1.771 (0.772)
0.6	1,286,246	279,427	838,281	97.44	2.27	0.30	1.779 (0.779)
0.7	900,008	198,155	594,465	97.11	2.52	0.37	1.791 (0.791)
0.8	656,437	146,480	439,440	96.53	3.01	0.46	1.803 (0.802)
0.9	500,340	112,600	337,800	96.17	3.27	0.57	1.815 (0.814)
1.0	392,476	89,285	267,855	95.50	3.80	0.71	1.831 (0.828)
1.1	314,556	72,188	216,564	95.21	4.00	0.79	1.839 (0.836)
1.2	258,660	59,829	179,487	95.16	3.97	0.88	1.841 (0.838)
1.3	216,783	50,539	151,617	94.92	4.10	0.98	1.839 (0.836)
1.4	187,470	44,005	132,015	94.79	4.19	1.02	1.832 (0.830)
1.5	161,769	38,193	114,579	94.63	4.19	1.18	1.832 (0.831)
1.6	138,700	33,234	99,702	94.17	4.53	1.31	1.838 (0.836)
1.7	120,996	29,198	87,594	94.25	4.40	1.35	1.834 (0.833)
1.8	106,709	25,993	77,979	93.83	4.55	1.62	1.841 (0.840)
1.9	95,912	23,550	70,650	93.72	4.60	1.69	1.847 (0.845)
2.0	85,111	21,097	63,291	93.09	5.09	1.82	1.861 (0.857)
2.5	57,916	14,687	44,061	89.96	7.07	2.98	1.934 (0.917)
3.0	56,557	13,663	40,989	90.25	6.64	3.10	1.933 (0.918)

TABLE IV- FF MESH FEATURES FOR TRABECULAR BONE

Mesh size (mm)	Number of Elements	Number of Nodes	NDOF	% Of Elements			AAR (SD)
				Good ($1 \leq AR < 2.5$)	Poor ($2.5 \leq AR < 3$)	Bad ($AR \geq 3$)	
0.5	895,874	186,394	559,182	97.55	2.24	0.21	1.777 (0.777)
0.6	607,507	127,292	381,876	97.44	2.31	0.25	1.780 (0.780)
0.7	438,098	92,292	276,876	97.43	2.32	0.25	1.780 (0.780)
0.8	329,495	69,935	209,805	97.32	2.39	0.28	1.783 (0.783)
0.9	255,407	54,544	163,632	97.23	2.43	0.35	1.784 (0.784)
1.0	201,233	43,382	130,146	97.05	2.53	0.42	1.787 (0.787)
1.1	163,118	35,391	106,173	96.63	2.84	0.53	1.799 (0.799)
1.2	137,293	29,946	89,838	96.82	2.65	0.53	1.788 (0.789)
1.3	113,397	24,901	74,703	96.71	2.73	0.56	1.794 (0.795)
1.4	98,677	21,909	65,727	96.28	3.07	0.64	1.801 (0.801)
1.5	85,019	18,957	56,871	96.11	3.07	0.81	1.805 (0.806)
1.6	73,931	16,644	49,932	95.61	3.45	0.94	1.816 (0.816)
1.7	64,553	14,678	44,034	95.52	3.39	1.09	1.816 (0.817)
1.8	58,092	13,278	39,834	95.06	3.77	1.17	1.827 (0.827)
1.9	50,930	11,790	35,370	94.82	3.88	1.30	1.835 (0.834)
2.0	46,182	10,762	32,286	94.46	4.07	1.47	1.840 (0.839)
2.5	31,783	7,651	22,953	92.23	5.62	2.15	1.887 (0.879)
3.0	26,616	6,511	19,533	92.93	4.91	2.17	1.875 (0.871)

TABLE V– FE MESH FEATURES FOR CARTILAGE

Mesh size (mm)	Number of Elements	Number of Nodes	NDOF	% Of Elements			AAR (SD)
				Good ($1 \leq AR < 2.5$)	Poor ($2.5 \leq AR < 3$)	Bad ($AR \geq 3$)	
0.5	273,338	66,942	200,826	97.69	2.07	0.24	1.774 (0.773)
0.6	168,500	43,223	129,669	96.77	2.79	0.44	1.774 (0.772)
0.7	113,956	30,083	90,249	94.20	4.81	1.00	1.863 (0.852)
0.8	81,753	22,209	66,627	92.04	6.75	1.21	1.939 (0.915)
0.9	60,560	17,052	51,156	91.05	7.50	1.45	1.976 (0.944)
1.0	46,078	13,437	40,311	89.12	9.11	1.77	1.988 (0.948)
1.1	37,138	11,113	33,339	87.86	9.60	2.53	1.986 (0.941)
1.2	30,204	9,272	27,816	88.47	8.72	2.81	1.960 (0.921)
1.3	25,128	7,871	23,613	88.81	8.21	2.98	1.946 (0.911)
1.4	21,552	6,888	20,664	89.97	7.29	2.74	1.929 (0.900)
1.5	18,629	6,048	18,144	90.60	6.84	2.56	1.933 (0.905)
1.6	16,726	5,463	16,389	91.31	6.44	2.25	1.934 (0.908)
1.7	14,648	4,858	14,574	91.66	5.97	2.37	1.955 (0.930)
1.8	13,074	4,386	13,158	91.02	6.59	2.39	1.978 (0.947)
1.9	11,896	4,024	12,017	90.20	7.52	2.28	1.999 (0.962)
2.0	10,956	3,719	11,157	87.67	9.43	2.90	2.046 (0.993)
2.5	8,076	2,775	8,325	74.96	17.32	7.71	2.216 (1.064)
3.0	7,208	2,467	7,401	65.77	19.63	14.59	2.356 (1.116)